Latin American Journal of Energy Research - Lajer
periodicos.ufes.br/lajer

Latin American Journal of Energy Research – Lajer (2024) v. 11, n. 2, p. 102–118
https://doi.org/10.21712/lajer.2024.v11.n2.p102-118

Sustainable biodiesel synthesis from oleic acid: kinetic study with carbonized bambara nutshell catalyst

Síntese sustentável de biodiesel a partir de ácido oleico: estudo cinético com catalisador bambara carbonizado

Haruna Mavakumba Kefas[1], Abdulhalim Musa Abubakar[1,*], Muhammad Jimada Aliyu[2], Raymond Bulus[1], Martin Stojchevski[3], Suhail Ahmed Soomro[4,5]

[1] Department of Chemical Engineering, Faculty of Engineering, Modibbo Adama University, Yola, Adamawa State, Nigeria
[2] Chemical Engineering Department, School of Infrastructure, Process Engineering and Technology, Federal University of Technology, Minna, Niger State, Nigeria
[3] Faculty of Technology and Metallurgy, Ss. Cyril and Methodius University in Skopje, North Macedonia
[4] Department of Chemical Engineering, Faculty of Engineering, Mehran University of Engineering & Technology Jamshoro, Pakistan
[5] Institute of Petroleum and Natural Gas Engineering, MUET, Jamshoro, Sindh, Pakistan
*Corresponding author E-mail: abdulhalim@mau.edu.ng

Received: 12 June 2024 | Accepted: 17 December 2024 | Published online: 26 December 2024

Abstract: Mineral content in bambara nutshell (BNS) can act as active sites for catalysis, while the protein content can be carbonized to produce support structures for the catalyst. BNS char based solid acid catalyst is produced in this study for biodiesel (FAME) production, using oleic acid esterified with methanol. The objective of the study is to determine the order of reaction ran at 50-65℃ for 180 min, utilizing the integral kinetic rate expression. It also involves analyzing the rate constants obtained, so as to use it to estimate the activation energy (E_a) and pre-exponential factors (k_O) necessary to describe the mechanism of the reaction. Findings show that, the presence of -OH functional group in BNS makes it a good candidate for biodiesel production. Faster reaction and conversion to FAME product (≅ 52%) occurred at 65℃. The first-order model almost describes the experimental data at 60℃ and R^2 = 0.9850, only that it has an intercept, which is not typical of the model; although not a sufficient reason to discard it. In this study, the best model fitted is second-order at the lowest temperature analyzed (i.e., 50℃ with rate constant, k_2 = 2× 10^5 L/mol.min), due to faster reaction rate described by its higher k_o value of 6.973× 10^5 L/mol.min. However, the first-order rate's low energy requirement (E_a = 51.63 kJ/mol), was the reason for its sluggishness compared to second-order E_a = 65.17 kJ/mol; which explains the reason why the choice of the best model could go both ways, if energy efficiency is considered. Despite the performance of the oleic acid, which is favorably described by the first- and second-order rate, its conversion to biodiesel is moderately significant.
Keywords: oleic acid; biodiesel production; bambara nutshell; free fatty acid; esterification.

Resumo: *O conteúdo mineral em poucas palavras bambara (BNS) pode atuar como sítios ativos para catálise, enquanto o conteúdo proteico pode ser carbonizado para produzir estruturas de suporte para o catalisador. O catalisador ácido sólido à base de carvão BNS é produzido neste estudo para produção de biodiesel (FAME), utilizando ácido oleico esterificado com metanol. O objetivo do estudo é determinar a ordem da reação executada a 50-65°C por 180 min utilizando a expressão da taxa cinética integral. Envolve também a análise das constantes de velocidade obtidas, de modo a utilizá-las para estimar a energia de ativação (E_a) e os fatores pré-exponenciais (k_o) necessários para descrever o mecanismo da reação. Os resultados mostram que a presença do grupo funcional -OH no BNS o torna um bom candidato para a produção de biodiesel. Reação e conversão mais rápidas em produto FAME (≅ 52%) ocorreram a 65°C. O modelo de primeira ordem quase descreve os dados experimentais a 60°C e R^2 = 0,9850, só que possui uma interceptação, o que não é típico do modelo; embora não seja uma razão suficiente para descartá-lo. Neste estudo, o melhor modelo ajustado é o de segunda ordem na temperatura mais baixa analisada (ou seja, 50°C com constante de taxa, k_2 = 2×10^5 L/mol.min), devido à taxa de reação mais*

rápida descrito por seu valor k_o mais alto de 6,973×10^5 L/mol.min. Entretanto, a baixa necessidade energética da taxa de primeira ordem (E_a = 51,63 kJ/mol), foi a razão de sua lentidão em relação à de segunda ordem E_a = 65,17 kJ/mol; o que explica a razão pela qual a escolha do melhor modelo pode ocorrer em ambos os sentidos, se for considerada a eficiência energética. Apesar do desempenho do ácido oleico, descrito favoravelmente pela taxa de primeira e segunda ordem, sua conversão em biodiesel é moderadamente significativa.
Palavras-chave: ácido oleico; produção de biodiesel; casca de noz bambara; ácido graxo livre; esterificação.

1 Introduction

Yadav et al. (2022) defined biodiesel or fatty acid methyl ester ($RCOOCH_3$, FAME), as a non-toxic, renewable, biodegradable and CO_2-neutral energy source. It is produced via esterification and/or transesterification process (Silva et al., 2019; Suwannakarn et al., 2009). Esterification process is the reaction between acids such as carboxylic acid or free fatty acid (FFA) with alcohol to produce ester and water. FAME production from renewable sources has gained significant attention in recent years due to its potential to reduce greenhouse gas emissions and dependence on fossil fuels. In this context, the utilization of oleic acid as a feedstock for biodiesel synthesis presents a promising avenue towards sustainable energy production. However, the efficient conversion of oleic acid into biodiesel faces challenges related to the kinetics of the reaction and the choice of suitable catalysts. Previous research efforts have explored various catalysts for biodiesel production, with studies by Mahdavi et al., (2015) highlighting the synthesis of biodiesel from oleic acid using zirconia/alumina (ZrO_2/Al_2O_3) nano-catalyst under high voltage conditions. Zubir (2009) utilized tungstated zirconia (WO_3/ZrO_2) to produce biodiesel from oleic acid, also developing kinetic model at 30-50℃ reaction temperature.

Patel et al. (2013) does the same using sulfated zirconia catalyst and tested the effect of several reaction parameters. Water adsorption apparatus and sulfuric acid catalyst was used by Lucena et al. (2008) to esterify oleic acid and methanol to manufacture FAME. Moradi et al. (2021) explored the application of a novel electrolysis approach for catalytic and non-catalytic synthesis of biodiesel using the same acid. Closest among previous research to the present one, was the manufacture or FAME by Kusmiyati & Sugiharto (2010) via reactive distillation. Notwithstanding, these studies have provided significant contributions to the process, but there is a need to further investigate the performance of the catalyst materials by carrying out kinetic study; so as to enhance the efficiency and sustainability of biodiesel synthesis. Together with response surface methodology optimization previously conducted by Maryam et al. (2021) and Han et al. (2019), the findings can be used to kick-start reactor design, solely for FAME production via esterification process.

Some biomass, such as bambara nut (*Vigna subterranea*) can be converted to esterification catalyst using simple technique. Bambara nut is a leguminous crop that is indigenous to Africa. Main factors that favor bambara nut as a suitable candidate for conversion to an esterification reaction catalyst are its high oil content, lipid profile, protein and mineral content, carbonaceous material and residual biomass utilization. In view of that, the present study focuses on the synthesis of biodiesel from oleic acid using a carbonized bambara nutshell (BNS) catalyst. Ibrahim et al. (2022) reported that catalysts normally employed are heterogeneous, namely: solid basic, solid acid and bifunctional acid-base type (viz., carbon-based, metal-based & polymer-based). Example is the areca nut husk, orange peel and watermelon peel derived heterogeneous catalyst, used by Yadav et al. (2022), Kumawat and Rokhum (2022) and Kushwaha et al. (2023), respectively.

Others include niobium acid, Amberlyst15, SAC-13, perfluorosulfonated, silica-alumina, sulfated zirconia, sulfated trioxide, sulfated titanium oxide, Smopex-101, ionomers, titania zirconia, zeolites of different types and photocatalyst (Abdulsalam and Farouk, 2020; Barange et al., 2021; Ghorbani-Choghamarani et al., 2022; Pang et al., 2021; Zubir, 2009). By means of exploring the kinetic aspects of the reaction and the catalytic properties of the BNS material, the research aims to address the challenges associated with sustainable biodiesel production from oleic acid. Also, via a detailed kinetic study, the authors sought to determine the most suitable reaction kinetic model for the experimental data that would be obtain, and gauge the speed and energy required to synthesize biodiesel by esterification. As such, a pretreated BNS sample was modified to act as a biocatalyst and characterized using Fourier Transform Infrared (FTIR) spectrometry. At the moment, similar study had been conducted using different acid, mode of operation, catalyst and reaction condition for first order rate expression (Silva et al., 2019), without

studying higher order rate of reactions. When a feasible process is achieved, the study will satisfactorily contribute to the advancement of green technology for renewable energy generation.

2 Methodology

2.1 Bambara nutshell pretreatment and carbonization

BNS was washed to remove the surface impurities and then placed in an air-blast drying oven at 105℃ to reduce its moisture content. A grinder was used to reduce its sizes and then sieved through 0.125 mm size sieve. About 18g BNS powder was put in a furnace under an inert nitrogen (N_2) atmosphere for 120-180 min at 300℃ to carbonize it, in a similar report by Oyedoh et al. (2022).

2.2 Carbon-based catalyst sulfonation

About 4g of BNS biochar was added to 100 mL of concentrated sulphuric acid (H_2SO_4) and heated in an oil bath between 75-135℃ sulfonation temperature (Faridi, 2017; Kumawat & Rokhum, 2022), simultaneously undergoing magnetic stirring for 300-480 min, under nitrogen flow. Sulfonate ions (RSO^{3-}) impurities were subsequently removed by diluting and washing the sample mixture with distilled water, as described by Rahma & Hidayat (2023). Adsorbed water molecules were removed by drying the sample at 105℃ in an oven for 720 min, and kept for further analysis.

2.3 FTIR characterization of the catalyst

Fourier Transform Infrared (FTIR-8400) instrument was used to detect the functional groups in RSO^{3-} catalyst.

2.4 Biodiesel production

To evaluate the catalytic activity of BNS-based heterogeneous catalyst, oleic acid was esterified using methanol in a 250 mL three-neck round-bottom flask undergoing magnetic stirring (Chongkhong et al., 2007; Zhang et al., 2023), which is equipped with a snake-like condenser set-up for methanol reflux. Methanol use was as reported by Patel et al. (2013).

An atmospheric pressure microwave reactor was employed to maintain the esterification temperature. Certain proportion of oleic acid, methanol and BNS-based heterogeneous acid catalyst was put inside a reactor to kick-start the esterification reaction, as carried out in Yadav et al. (2022).

When the specific reaction time was attained, the BNS-based heterogeneous acid catalyst was separated from the product mixture via filtration, and the generated water and excess methanol removed via vacuum distillation. Next, the catalytic performance of the BNS-based heterogeneous acid catalyst (% conversion) were then calculated in accordance with the GB 5009.229-2016 standard method.

2.5 Esterification reaction kinetics

A set of experiment was carried out using the optimum conditions for the conversion. They are 3 wt.% catalyst dose, 10:1 methanol-oleic acid molar ratio (Moradi et al., 2021), 600 rpm stirring speed < 800 rpm used in Naeem et al. (2021) and 3 h reaction time – varied accordingly, taking 1, 5, 10, 30, 60, 90, 100, 110, 130, 150 and 180 min.

The experiment was conducted at different reaction temperatures of 50, 55, 60 and 65℃ in a three-neck conventional reflux batch reactor. Both time and temperature range specification employed was according to Sawitri and Budiman (2016). Approximately 7 mL of sample was taken out of the reactor after every reaction time interval in a centrifuge tube, and iced to finally stop the reaction. In essence, the product was separated from the mixture and the FFA of the product plus that of the feedstock was determined using the AOCS Ca 5a-40 procedure (Ibrahim et al., 2022), following Eq. (1). Following this was the calculation of the % FFA conversion using Eq. (2) (Rahma and Hidayat, 2023).

$$\text{FFA value} = \frac{(\text{Titre value}) \times (0.1\text{N NaOH}) \times 28.2}{\text{Weight of Sample}} \quad (1)$$

$$\%\ \text{FFA Conversion} = \frac{(\text{FFA value of Feedstock}) - (\text{FFA value of Product})}{(\text{FFA value of Feedstock})} \times 100 \quad (2)$$

FFA value also imply FFA concentration. Herein, the esterification reaction conducted was based on Reaction 3, where FFA reacts with CH_3OH to form FAME and water (Nata et al., 2017), using oleic acid as homogeneous catalyst.

$$RCOOH + CH_3OH \rightleftharpoons RCOOCH_3 + H_2O \quad (3)$$

Narkhede and Patel (2013) state that the esterification of oleic acid is an equilibrium-limited reaction. In order to overcome the equilibrium limitation, the reaction was carried out by taking alcohol in excess. Kinetics was then performed to determine the reaction rate and rate constant, k, required for converting FFA to biodiesel at the respective temperatures examined, based on a presumed order of reactions, $n = 1$, 2 and 3. Rate constants, k_1, k_2 and k_3 corresponding to the respective reaction orders were then calculated, following the steps examined herein.

2.5.1 Reaction rate constant

Pseudo-homogeneous model of first, second and third-order reaction given by Eqs. (4), (5) and (6) (Rani et al., 2020), respectively, were transformed.

$$-r_A = k_1 C_{FFA} C_M = k_1 C_{FFA} \quad (4)$$

$$-r_A = k_2 {C_{FFA}}^2 \quad (5)$$

$$-r_A = k_3 {C_{FFA}}^3 \quad (6)$$

Where, $-r_A$ = rate of reaction of FFA, C_{FFA} = FFA concentration and C_M = methanol concentration. But since, C_M is assumed fixed, the first-order reaction rate was presented in pseudo-form (Equation 1). An integral version of Eqs. (3)-(5), consistent with Eqs. (7)-(9) (Taufiq et al., 2018), was then used to determine k_n, where C_{FFA_0} = initial FFA value or concentration of the feedstock.

$$-\ln\left(\frac{C_{FFA}}{C_{FFA_0}}\right) = k_1 t \quad (7)$$

$$\frac{1}{C_{FFA}} = \frac{1}{C_{FFA_0}} + k_2 t \quad (8)$$

$$\frac{1}{{C_{FFA}}^2} = \frac{1}{{C_{FFA_0}}^2} + 2k_3 t \quad (9)$$

From the slope of a linear plot of the dependent versus independent terms/variables in Equations 7-9, k_1, k_2 and k_3 were computed for each reaction temperature. The order of reaction or rate kinetics that best fit the empirical concentration and time data after the plot was later chosen as the best model, and hence the corresponding order was selected as the order of reaction.

2.5.2 Activation energy determination

The k_n's' and the temperature were correlated by the Arrhenius model, given by Eq. (10). From the linearized form of Equation 10 (i.e., Eq. 11), activation energy (E_a) and the pre-exponential factor (k_o), was estimated (Kumawat and Rokhum, 2022; Zhang et al., 2017).

$$k_n = k_o\, e^{-E_a/RT} \quad (10)$$

$$\ln k_n = \ln k_o - \frac{E_a}{R}\left(\frac{1}{T}\right) \quad (11)$$

Explicitly, a plot of $\ln k_n$ against $\frac{1}{T}$ was carried out, taking molar gas constant, R, as 8.314 J/mol.K and T = absolute temperature (K).

3 Results and discussion

3.1 FTIR functional group

Peaks for the BNS catalyst and char, representing the functional groups present, were displayed in Figures 1 and 2. Higher peak heights suggest a higher concentration or stronger presence of those functional groups. On the other hand, the changes in wavenumbers can indicate variations in the chemical bonds or structures present in the catalyst and char.

In Figure 1, the peak 607.3859 cm^{-1} points to the possible presence of alkenes functional group. The presence of such unsaturated hydrocarbons can participate in catalytic reactions involving double bonds.

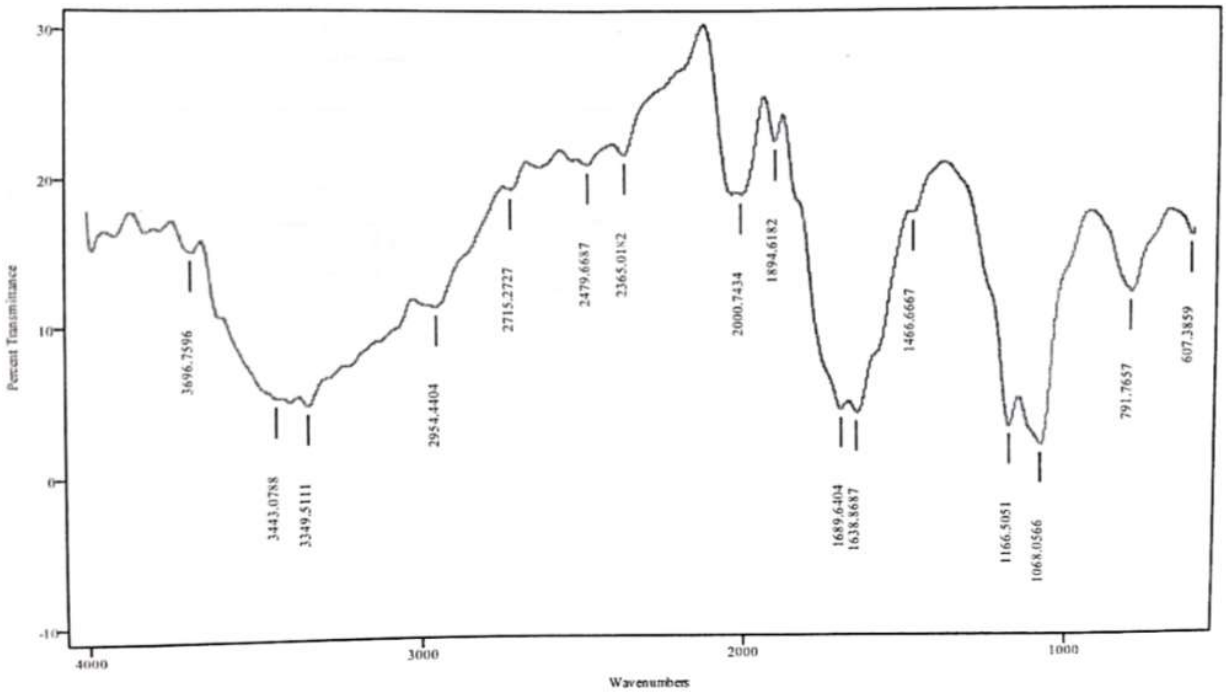

Figure 1. Functional group trend after FTIR analysis of Bambara nut catalyst.

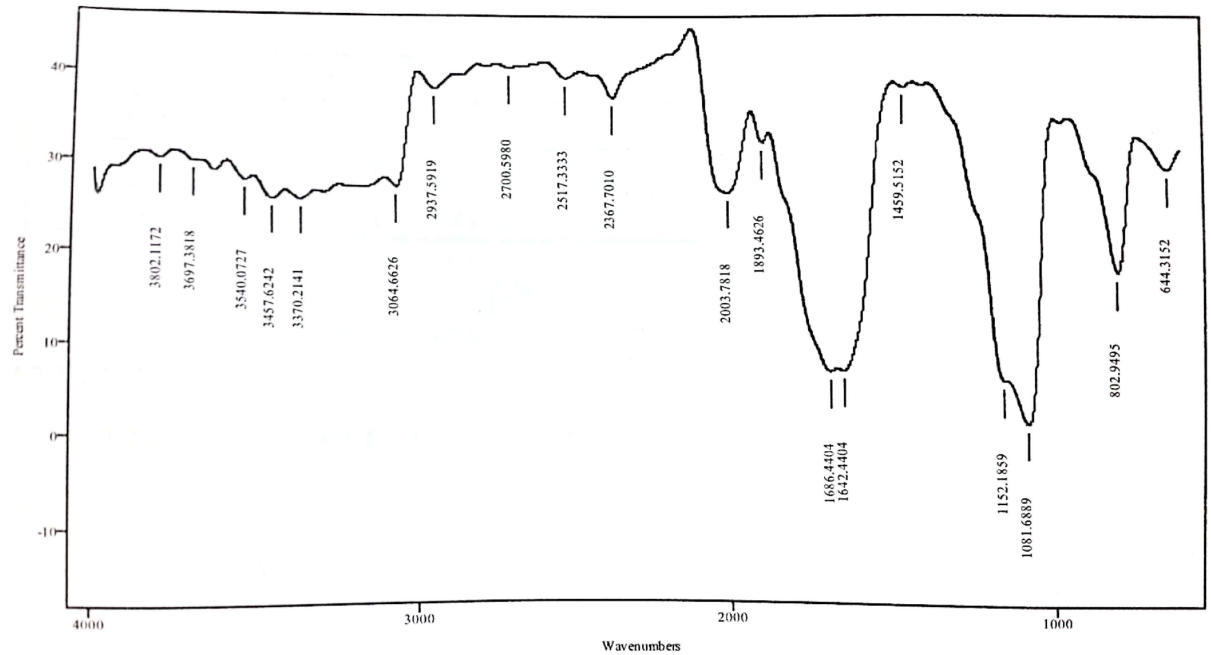

Figure 2. Functional group trend after FTIR analysis of Bambara nut char.

Also, peak at 1466.6667 cm^{-1} demonstrate the possible presence of alkene functional group, which can enhance catalytic properties. A peak = 791.7657 cm^{-1} represents an alcohol presence. Hydroxyl groups can act as catalyst sites for esterification reactions in biodiesel production (Abdulsalam & Farouk, 2020). Catalytic activity is also enhanced by the presence of additional alcohol functional group at a peak of 1894.6182 cm^{-1}. Aromatic compounds are the possible functional group present as a result of the peak of 1068.0566 cm^{-1}, whose structure may contribute to the catalytic activity of the catalyst. At a peak of 1638.8687 cm^{-1}, ethers play a role in the catalytic conversion of reactants in biodiesel production. In Figure 2, the continued presence of unsaturated hydrocarbons in the char material, indicates the presence of alkene functional group at a peak of 644.3152 and 1459.5152 cm^{-1}.

Peak at 1081.6889 and 1893.4626 cm^{-1} in Table 1, signifies alcohol presence in the char (Faridi, 2017); those corresponding to 802.9495 cm^{-1}, points to the likelihood of aromatic compound presence, and; 1642.4404 cm^{-1} wavenumber, is consistent with the presence of ethers, all influencing the char catalytic property. The finding was partly in agreement with Abdulsalam & Farouk (2020) who reported that a solid acid catalyst must possess carboxylic acid (-COOH), sulfonic acid ($-SO_3H$) and hydroxyl (-OH) functional groups for it to be efficient. It is basically due to the fact that both the bambara nut catalyst and char exhibit peaks that could correspond to the presence of carboxylic acid (-COOH) groups (Table 1), particularly the C=O stretch around 1690 cm^{-1} and broad O-H stretches around 2700-2950 cm^{-1}. Whereas, the presence of -SO3H groups is less certain.

Although there are peaks that could correspond to the S=O symmetric stretch (~1150-1170 cm^{-1}), the absence of clear peaks around 1375-1390 cm^{-1} for the S=O asymmetric stretch makes it difficult to definitively confirm the presence of sulfonic acids.

Table 1. FTIR percent transmittance versus wavenumber of BNS catalyst and char.

Bambara Nut Catalyst		Bambara Nut Char	
Wavenumbers	Peak Height	Wavenumbers	Peak Height
607.3859	16.2080	644.3152	30.0407
791.7657	12.4055	802.9495	18.6512
1068.0566	1.8971	1081.6889	1.9842
1166.5051	3.2166	1152.1859	6.6879
1466.6667	17.7797	1459.5152	39.0757
1638.8687	4.1292	1642.4404	7.6927
1689.6404	4.3910	1686.4404	7.6571
1894.6182	22.5008	1893.4626	33.0378
2000.7434	18.9799	2003.7818	27.4724
2365.0182	21.6032	2367.7010	37.9632
2479.6687	20.9941	2517.3333	40.1630
2715.2727	19.3499	2700.5980	41.2734
2954.4404	11.4821	2937.5919	38.9231
3349.5111	4.7824	3064.6626	27.9120
3443.0788	5.2493	3370.2141	26.3468
3696.7596	15.1767	3457.6242	26.2698
-	-	3540.0727	28.2868
-	-	3697.3818	30.2229
-	-	3802.1172	30.3753

Some lower and higher transmittance at those peaks and corresponding with the stated functional groups in the char and catalyst, demonstrates the absorption of significant number of infrared rays. Specifically, transmittance of 17.7797 and 22.5008% for the catalyst and 30.0407, 39.0757 and 33.0378% for the char, allows more infrared radiation to pass through.

3.2 FFA conversion

Data used for this kinetic study were obtained from the calculated FFA value of the OFA converted to FAME. This FFA concentrations are showcased in Table 2 at 50-65℃ and were the one employed in the determination of the % FFA conversions using Equation 2, as observed in Taufiq et al. (2018).

Table 2. FFA value at different temperature.

Time (min)	FFA Concentration (mmol/L)			
	50℃	**55**℃	**60**℃	**65**℃
1	91.78	92.95	93.54	95.3
5	89.06	89.45	89.04	89.8
10	86.34	85.95	84.54	84.3
30	83.62	82.45	80.04	78.8
60	80.9	78.95	75.54	73.3
90	78.18	75.45	71.04	67.8
110	75.46	71.95	66.54	62.3
130	72.74	68.45	62.04	56.8
150	70.02	64.95	57.54	51.3
180	67.3	61.45	53.04	45.8

As it is, C_{FFA_0} = 91.78, 92.95, 93.54 and 95.30 mmol/L (Table 2) are the starting concentration at 1 min. A gradual and consistent decrease in FFA value was expected from these initial values at the set temperature value. A clearer depiction of C_{FFA_0}-time relationship is shown in Figure 3.

It is observed that the concentration decreasing rate is almost same (0.205 mmol/L/min), arriving at a final mean C_{FFA} value of 56.8975 mmol/L. In the esterification reaction experiment, FFA concentration decreases with time as the reaction progresses (Nata et al., 2017), as shown in Figure 3. This decrease in concentration is due to the consumption of the reactants to form products. At this juncture, it is difficult to gauge the influence of temperature rise or change in the esterification reaction, as Figure 3 presents the same trend.

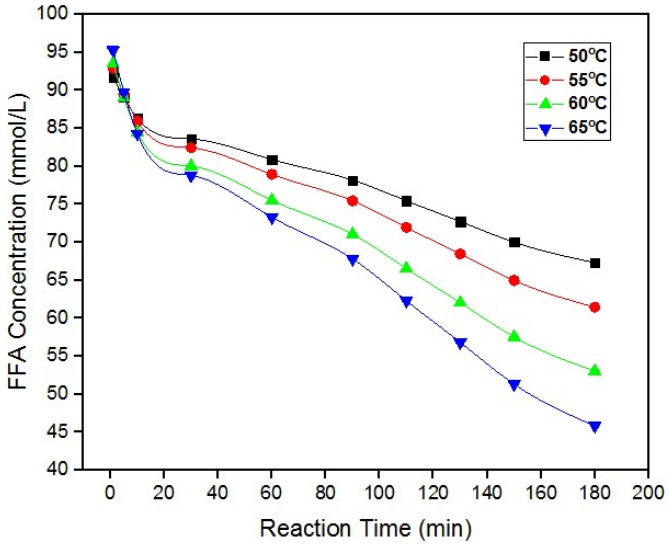

Figure 3. Change in FFA concentration with time.

But it is known that, increasing the temperature (viz., 50-65℃) would possibly lead to an increase in the reaction rate due to the higher kinetic energy of the molecules (Rani et al., 2020). This increased kinetic energy result in more frequent and energetic collisions between reactant molecules, leading to a higher likelihood of successful collisions and product formation. At higher temperatures, the reaction rate is usually faster, which resulted in a more rapid decrease in FFA concentrations over time (e.g., 95.3-45.8 mmol/L at 65℃), compared to reactions at lower temperatures.

Basically, the slope of the curves in Figure 3 indicates the rate at which the FFA value is decreasing. Steeper slopes of the 60 and 65℃ curves, suggest a faster decrease in concentration, respectively having an average decreasing rate of 0.207 and 0.218 mmol/L/min. Table 2 contains the required variables to calculate or determine the % FFA conversion $\left(\frac{C_{FFA_0}-C_{FFA}}{C_{FFA_0}} \times 100\right)$, which is originally based on Equation 2. For simplicity, % FFA conversion is represented with the symbol X_{FFA}, as shown in Table 3.

Table 3. Computed FFA conversion at various time and specific temperature.

Time (min)	X_{FFA}			
	50°C	55°C	60°C	65°C
1	0	0	0	0
5	0.029636	0.037655	0.048108	0.057712
10	0.059272	0.075309	0.096216	0.115425
30	0.088908	0.112964	0.144323	0.173137
60	0.118544	0.150619	0.192431	0.23085
90	0.14818	0.188273	0.240539	0.288562
110	0.177817	0.225928	0.288647	0.346275
130	0.207453	0.263583	0.336754	0.403987
150	0.237089	0.301237	0.384862	0.4617
180	0.266725	0.338892	0.43297	0.519412

Table 3 provides a snapshot of the efficiency of the esterification reaction in converting FFA to biodiesel at each time point. In this study, a higher temperature of 65°C lead to faster (effective) conversion rates due to increased reaction kinetics, with an efficiency clocking 51.94% at the end of the process (i.e., 180 min). By implications, the optimal temperature conditions for maximizing FFA conversion in biodiesel production is 65°C, as obtained in the present study. Although, high range between 70-100°C was previously studied by Chongkhong et al. (2007).

The increasing X_{FFA} with time (Figure 4), also obtained by Rahma & Hidayat (2023) for 30, 40, 50 and 60°C and Sawitri & Budiman (2016) for 50-65°C, advocates that the esterification reaction is proceeding effectively and converting FFA molecules into biodiesel products. The rate of conversion may vary at different time intervals, reflecting the kinetics of the reaction.

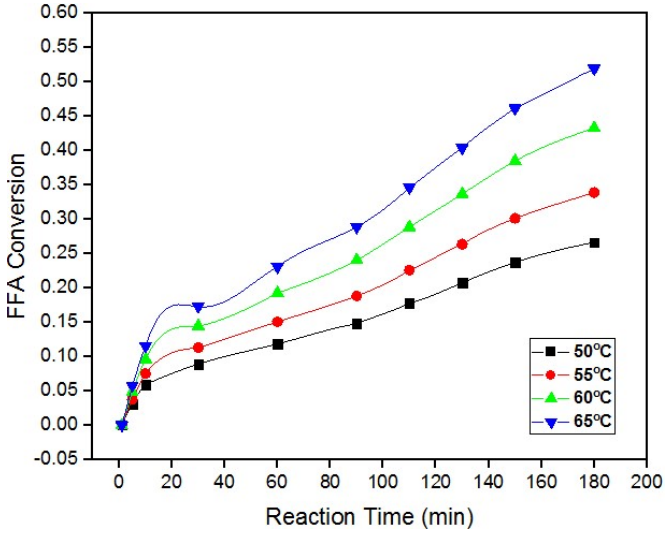

Figure 4. FFA fractional conversion variation with reaction time.

Considering the data presented in Table 3 and the trend of increasing X_{FFA} with temperature and time in Figure 4, it is reasonable to consider discarding the temperature of 50°C for achieving higher FFA conversion rates within the same time frame. Maafa (2022) affirmed the behavioral trend of Figure 3 and 4 in a single plot, affirming that 70°C is the optimum temperature for FFA conversion in his study.

3.3 Kinetic study deductions

Based on n = 1, 2 and 3 reaction rate equations linearized to Equations 6-8 via integral method, dependent parameters values in Table 4 were determined and displayed for all the temperatures studied. It is observed that the values of $-\ln\left(\frac{C_{FFA}}{C_{FFA_0}}\right)$ at each temperature appear to increase linearly with time, suggesting that the reaction might be first-order. Also, the values of $\frac{1}{C_{FFA}}$ for each temperature also show an increasing trend

with time, suggesting the possibility of second-order kinetics. At the same time, the data under n = 3 doesn't immediately suggest a third-order reaction.

Table 4. Computed values for kinetic data graphing and rate constant determination.

Temperature	50℃	55℃	60℃	65℃
Time (min)	$-\ln\left(\frac{C_{FFA}}{C_{FFA_0}}\right)$	$-\ln\left(\frac{C_{FFA}}{C_{FFA_0}}\right)$	$-\ln\left(\frac{C_{FFA}}{C_{FFA_0}}\right)$	$-\ln\left(\frac{C_{FFA}}{C_{FFA_0}}\right)$
First Order:				
1	0	0	0	0
5	0.030084	0.038382	0.049303	0.059445
10	0.061101	0.078296	0.101164	0.122648
30	0.093112	0.11987	0.155863	0.190117
60	0.126181	0.163247	0.213727	0.262469
90	0.160381	0.208592	0.275146	0.340468
110	0.195792	0.25609	0.340586	0.425068
130	0.232503	0.305958	0.41061	0.517493
150	0.270613	0.358444	0.485909	0.619339
180	0.310234	0.413838	0.567343	0.732746
Time (min)	$\frac{1}{C_{FFA}}$ (L/mmol)	$\frac{1}{C_{FFA}}$ (L/mmol)	$\frac{1}{C_{FFA}}$ (L/mmol)	$\frac{1}{C_{FFA}}$ (L/mmol)
Second Order:				
1	0.010896	0.010758	0.010691	0.010493
5	0.011228	0.011179	0.011231	0.011136
10	0.011582	0.011635	0.011829	0.011862
30	0.011959	0.012129	0.012494	0.01269
60	0.012361	0.012666	0.013238	0.013643
90	0.012791	0.013254	0.014077	0.014749
110	0.013252	0.013899	0.015029	0.016051
130	0.013748	0.014609	0.016119	0.017606
150	0.014282	0.015396	0.017379	0.019493
180	0.014859	0.016273	0.018854	0.021834
Time (min)	$\frac{1}{C_{FFA}^2}$ (L/mmol)^2	$\frac{1}{C_{FFA}^2}$ (L/mmol)^2	$\frac{1}{C_{FFA}^2}$ (L/mmol)^2	$\frac{1}{C_{FFA}^2}$ (L/mmol)^2
Third Order:				
1	0.000119	0.000116	0.000114	0.00011
5	0.00012	0.000117	0.000116	0.000111
10	0.000127	0.00012	0.000119	0.000114
30	0.000131	0.000127	0.00012	0.000116
60	0.000134	0.000129	0.000124	0.000119
90	0.000136	0.000132	0.00013	0.000124
110	0.000163	0.000158	0.000139	0.000128
130	0.00019	0.000175	0.000162	0.000139
150	0.000236	0.000221	0.000207	0.000153
180	0.000284	0.000249	0.000241	0.00018

Figures 5-7 shows the kinetic plots carried out to determine *k* and gauge the performance of the catalyst at the chosen temperatures. For a reaction following first-order kinetics, a plot of $-\ln\left(\frac{C_{FFA}}{C_{FFA_0}}\right)$ versus time yields a straight line, as shown in Figure 5.

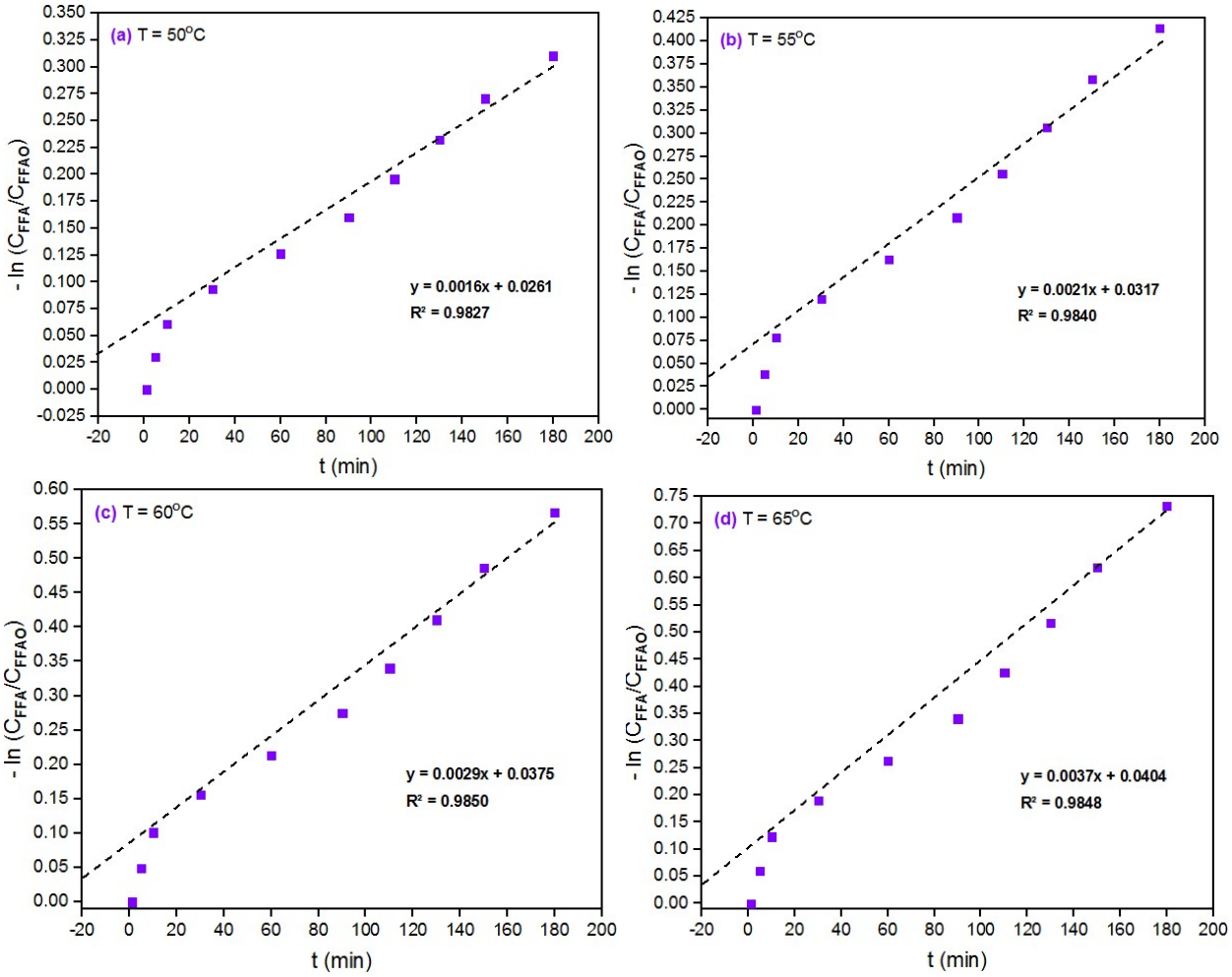

Figure 5. First order reaction rate plot at various temperatures.

Coefficient of determination, R^2 value close to 1 in Figures 5-6 indicates that the data points lie close to the regression line at 50-65℃, suggesting that the reaction follows first- and second-order kinetics. In Figure 5, it infers that the concentration of FFA decreases exponentially over time, which is the characteristic of first-order reactions.

Consistently high R^2 values across all temperatures (i.e., 0.9827, 0.9840, 0.9850 & 0.9848) suggest that the reaction mechanism does not change with temperature and that the first-order kinetic model is robust for describing this reaction. Because the 60℃ line gives the highest value, it appears to be the one that best described the synthesis process. Nonetheless, a deviation of concern in the behavior of the plot in Figure 5, is the existence of an intercept, which is not what was portrayed by Equation 6.

Side reactions or intermediate steps, instrumental or experimental errors, non-ideal behavior and C_{FFA_0} measurement error, are potential causative reasons for this deviation. Therefore, some initial delay in the reaction that isn't accounted for exist, resulting in the plot not starting exactly at zero. The presence of an intercept can be attributed to several factors as mentioned earlier, such as non-ideal behavior, but it does not necessarily invalidate the first-order kinetics model. Similarly, a second-order reaction plot of $\frac{1}{C_{FFA}}$ versus time in Figure 6 was linear, indicating that the reaction rate is proportional to the square of the FFA concentration.

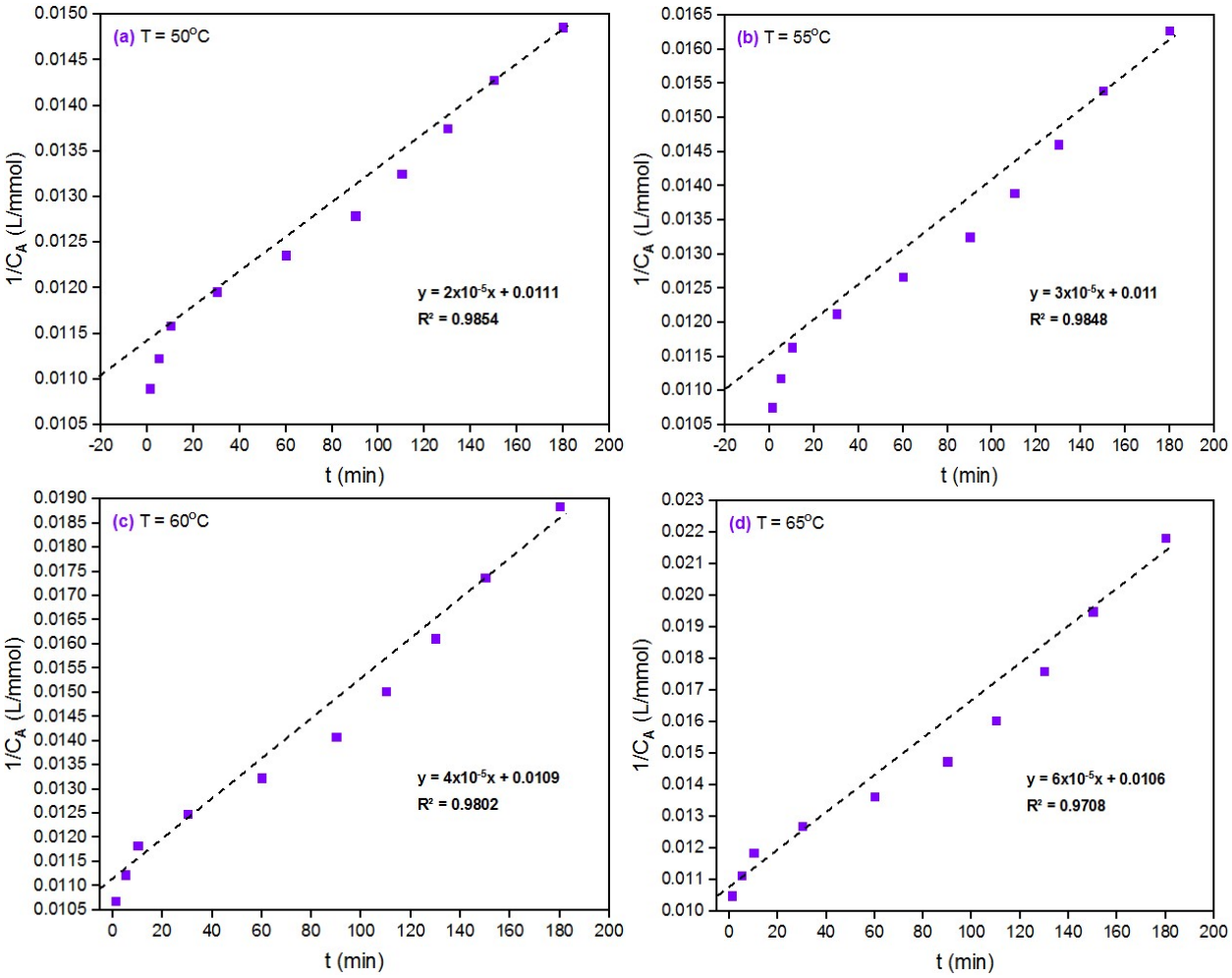

Figure 6. Second order reaction rate plot at various temperatures

Even if the first-order plot (Figure 5) shows an intercept, indicating some deviation, the linear behavior and high R^2 values in the second-order plot (Figure 6) support that the second-order model is appropriate for describing the reaction kinetics. This consistency across different temperatures reinforces the suitability of the second-order reaction model, above the first-order kinetics. Basically, the highest R^2 value = 0.9854 is at 50°C, showing that the second-order reaction model best fits the data at this temperature.

In Figure 6, the R^2 values demonstrated that the extent of fit decreases with increasing temperature. The efficiency of the BNS catalyst used in the reaction might decrease at higher temperatures, affecting the overall reaction rate and causing poorer fit. There might also be changes in the physical state of the reactants or the catalyst (e.g., evaporation, decomposition) at higher temperatures, affecting the reaction kinetics. In Figure 7, it is observed that the data points are more scattered due to lower R^2 values ranging from 0.7875-0.8454 recorded at all temperatures for third-order kinetics of the esterification reaction.

There is obviously an equal and consistent intercept value = 0.0001 for all temperatures plotted for the third-order rate. Equal intercept values suggest that the experiments were conducted under very consistent initial conditions. This enhances the reliability of the comparison of reaction rates across different temperatures. In addition, the slope of each line is proportional to k_3. Higher slopes indicate higher k_3, implying a faster reaction rate at that temperature. With consistent initial conditions, any differences observed in the slopes of the plots (8×10^{-7}, 7×10^{-7}, 6×10^{-7} and 3×10^{-7} $L^2/mmol^2.min$) can be attributed more confidently to changes in k_3 due to temperature variations, rather than discrepancies in C_{FFA_0}. Figure 7 suggests that the reaction does not perfectly adhere to third-order kinetics across the temperatures studied, with moderate R^2 values indicating some degree of fit. The best fit is observed at 65°C, implying that the reaction exhibits more consistent third-order behavior at this temperature, though not ideally so.

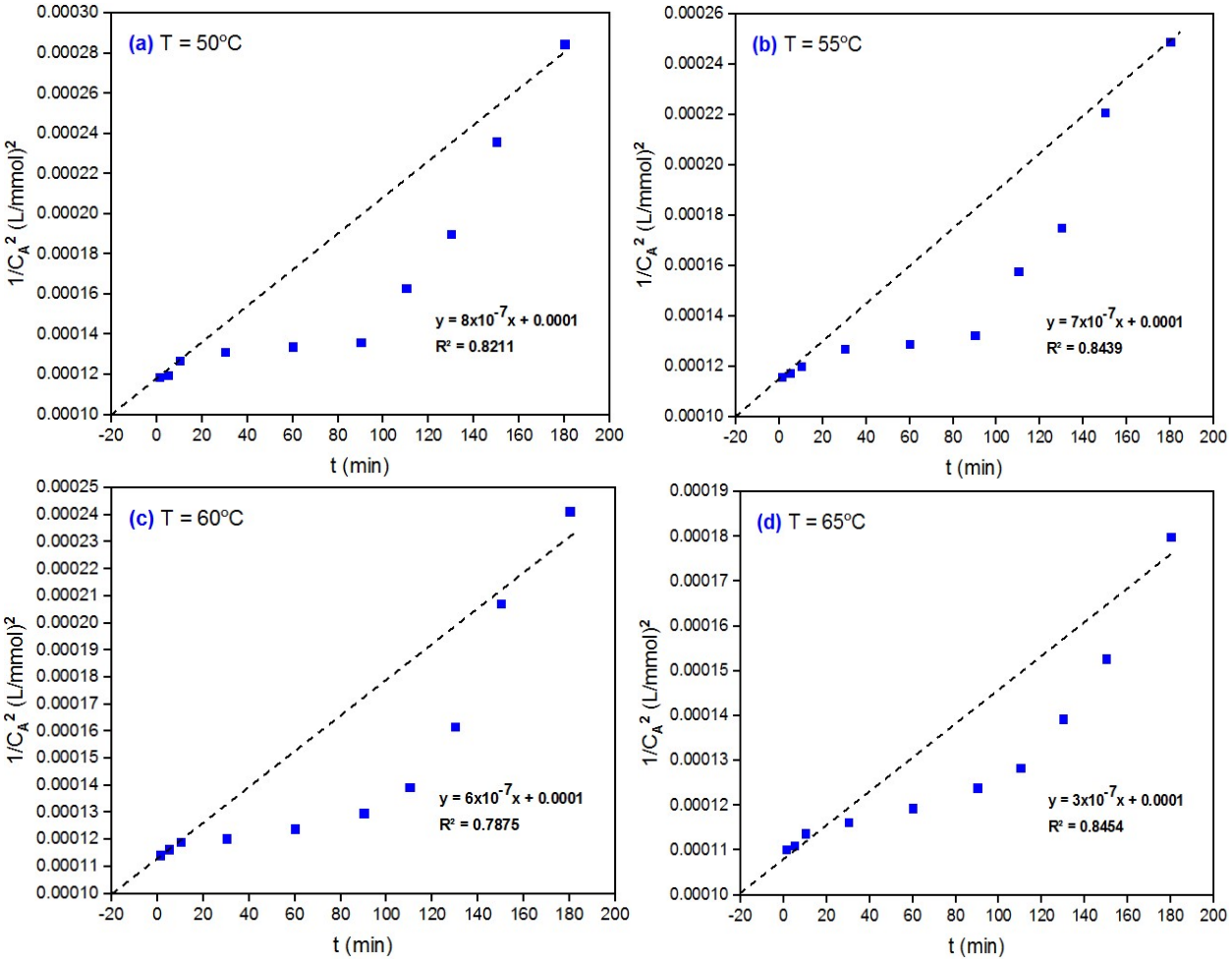

Figure 7. Third order reaction rate plot at various temperatures

3.4 Inference from Arrhenius parameters

Based on the order of reaction, a plot of '$\ln k_n$' against '$\frac{1}{T}$', which is known as the Arrhenius plot, gives the pre-exponential factor, k_o and the activation energy, E_a. Using the data in Table 5, k_1, k_2 and k_3 from the slopes of the plots shown in Figures 5-7 helped in the estimation of the Arrhenius parameters for each reaction order.

As the temperature increases at n = 1 and n = 2, the slope of the line (rate constant, k) also increase, as mentioned by Taufiq et al. (2018), indicating that the reaction proceeds faster at higher temperatures. It also confirms that the reaction follows both first- and second-order kinetics only.

Table 5. Kinetic data for activation energy determination.

n=1					
T (°C)	**T(K)**	$\frac{1}{T}$ **(K^{-1})**	$\frac{1}{T} \times 10^{-3}$ **(K^{-1})**	k_1 **(min^{-1})**	$\ln k_1$
50	323	0.003096	3.096	0.0016	-6.43775
55	328	0.003049	3.049	0.0021	-6.16582
60	333	0.003003	3.003	0.0029	-5.84304
65	338	0.002959	2.959	0.0037	-5.59942
n=2					
T (°C)	**T(K)**	$\frac{1}{T}$ **(K^{-1})**	$\frac{1}{T} \times 10^{-3}$ **(K^{-1})**	k_2 **(L/mol.min)**	$\ln k_2$
50	323	0.003096	3.096	2×10^{-5}	-10.8198
55	328	0.003049	3.049	3×10^{-5}	-10.4143
60	333	0.003003	3.003	4×10^{-5}	-10.1266
65	338	0.002959	2.959	6×10^{-5}	-9.72117

n=3					
T (℃)	**T(K)**	$\frac{1}{T}$ **(K^{-1})**	$\frac{1}{T} \times 10^{-3}$ **(K^{-1})**	k_3 **(L^2/mol^2.min)**	**ln k_3**
50	323	0.003096	3.096	4×10^{-7}	-14.7318
55	328	0.003049	3.049	3.5×10^{-7}	-14.8653
60	333	0.003003	3.003	3×10^{-7}	-15.0195
65	338	0.002959	2.959	1.5×10^{-7}	-15.7126

Figures 8-10 are Arrhenius plot for n = 1, 2 and 3, respectively, depicting a graph of ln k_n against $\frac{1}{T}$ (Naeem et al., 2021). Promising estimates of E_a and k_o can be realized in Figures 8 and 9 at n = 1 and 2 due to their high R^2 fit values of 0.9980 and 0.9952, respectively. Coupled with the identical trend observed, the first- and second-order kinetic equation fit the empirical data for the biodiesel production far better than the third-order model.

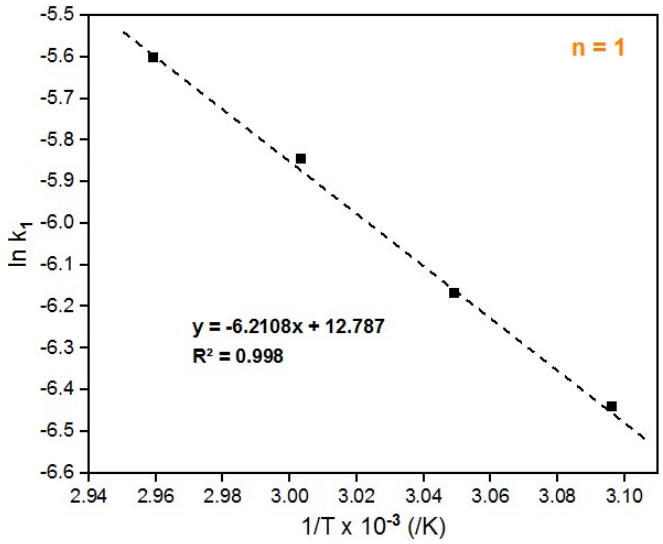

Figure 8. Arrhenius plot based on presumed reaction order of 1.

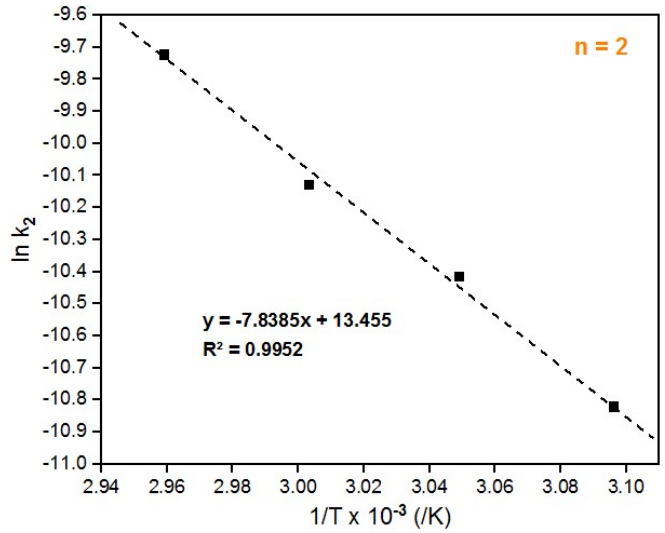

Figure 9. Arrhenius plot based on presumed reaction order of 2.

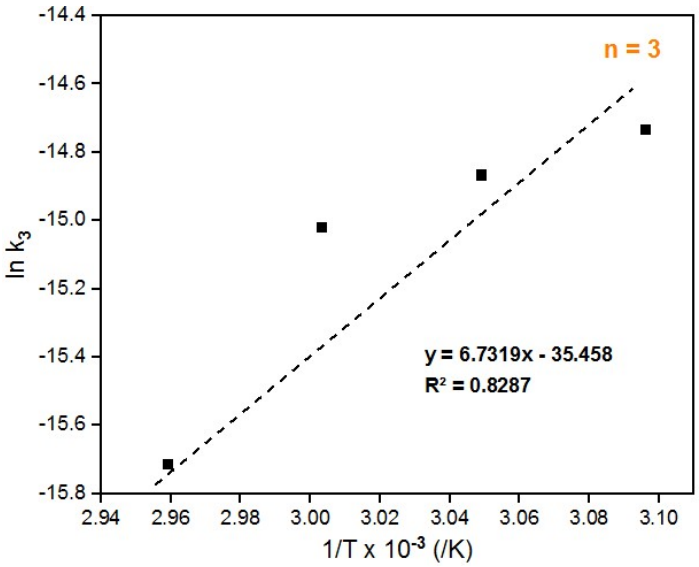

Figure 10. Arrhenius plot based on presumed reaction order of 3.

The fact that $\ln k_3$ increases with an increase in $\frac{1}{T}$ (Figure 10), suggests that k_3 increases with a decrease in temperature. This behavior contradicts the typical Arrhenius equation where k increases with increasing temperature, and $\ln k_n$ decreases when $\frac{1}{T}$ is increasing (Cardoso et al., 2008). Evidently, the third-order rate kinetics is not supported by the Arrhenius model. Simply because $R_1^2 > R_2^2$ and $R_1^2 > R_3^2$, which shows that the first-order model provides the best fit, as contained in Table 6, followed by n = 2.

Table 6. Activation Energy and Pre-exponential Factors.

Order	Parameter	Value
n = 1	E_a (kJ/mol)	51.63659
	k_o (min^{-1})	3.575×10^5
	R^2	0.9980
n = 2	E_a (kJ/mol)	65.16929
	k_o (L/mol.min)	6.973×10^5
	R^2	0.9952
n = 3	E_a (kJ/mol)	–55.96902
	k_o (L^2/mol^2.min)	3.988×10^{-16}
	R^2	0.8287

Thus, the E_a of 51.64 and 65.17 kJ/mol represents the minimum energy required for the reactant molecules to undergo the necessary collision and form the products. A lower E_a at n =1 suggests that the reaction proceeds more readily, as it requires less energy to overcome the energy barrier. In a second order reaction, the E_a of 65.16929 kJ/mol indicates a higher energy barrier compared to the 1st order reaction. This suggests that the reaction requires more energy for the molecules to overcome the E_a barrier and proceed to form the biodiesel product.

As desired, the E_a for the best fit rate model (n = 1 & 2) falls within the range of 42-74.4 kJ/mol reported for oleic acid exploration in several studies by Narkhede & Patel (2013). In general, E_a values cannot be negative as they represent the energy barrier for the reaction. Negative values (say, –55.969 kJ/mol in Table 6) could arise from computational errors or inaccuracies in the experimental data, as in n = 3, obtained in this study. Higher value of k_o at n = 2 (6.973×10^5 L/mol.min) indicate a higher frequency of collisions and thus a faster reaction rate, whereas lower value at n = 1 (3.575×10^5 min^{-1}) suggest less frequent collisions and a slower reaction rate. The value of $k_o = 3.988 \times 10^{-16}$ L^2/mol^2.min indicates a very low frequency of successful collisions for the third-order reaction, which is typical for higher-order reactions.

4 Conclusion

A higher proportion of unsaturated fatty acids like oleic and linoleic acids improves the fluidity and quality of biodiesel, which is also contained in BNS. The production of biodiesel using BNS catalyst in this study, was successfully achieved by pretreating and carbonizing the BNS solid catalyst, characterizing it for specific functional group presence, determining the FFA concentration and conversion to FAME, and the studying of the kinetics and thermodynamic of the process. It was achieved by studying the % FFA conversion at 50, 55, 60 and 65℃ using 10:1 methanol-oleic acid molar ratio. By fitting the kinetic data to first-, second- and third-order reaction rate models, it was discovered that the second order model best describe the empirical findings, followed by the first order model; while the third-order model deviates completely.

Oleic acid used as the FFA, aided in the production of moderate amount of biodiesel. To improve the third-order fit, broader analysis of more specific temperature range to identify any patterns or specific conditions where the reaction follows the expected kinetics more closely, is recommended. Utilization of advanced data analysis techniques to account for potential side reactions or changes in the BNS catalyst activity is also recommended.

Conflicts of interest

There is no conflict of interest between the authors and the respective institutions.

Research and publication ethics

The study was carried out within the rules of research and is within the scope of LAJER. Publication ethics were followed during the paper preparation.

Acknowledgement

Raymond Bulus with B.Eng. in Chemical Engineering, wishes to appreciate his Supervisors for the guidance during his B.Eng. Research Project at Modibbo Adama University. We collectively acknowledge the insight from all participating authors towards the publication of this manuscript.

Bibliographic References

Abdulsalam, M., & Farouk, H. U. (2020). Synthesis of fatty acid methyl ester (biodiesel) using environmentally benign catalyst (yam peel). ChemSearch Journal (CSJ), 11(2), 15–23. http://www.ajol.info/index.php/csj

Barange, S. H., Raut, S. U., Bhansali, K. J., Balinge, K. R., Patle, D. S., & Bhagat, P. R. (2021). Biodiesel production via esterification of oleic acid catalyzed by Brønsted acid-functionalized porphyrin grafted with benzimidazolium-based ionic liquid as an efficient photocatalyst. Biomass Conversion and Biorefinery, 13, 1873–1888. https://doi.org/10.1007/s13399-020-01242-7

Cardoso, A. L., Neves, S. C. G., & da Silva, M. J. (2008). Esterification of oleic acid for biodiesel production catalyzed by SnCl2: A kinetic investigation. Energies, 1, 79–92. https://doi.org/10.3390/en1020079

Chongkhong, S. Ã., Tongurai, C., Chetpattananondh, P., & Bunyakan, C. (2007). Biodiesel production by esterification of palm fatty acid distillate. Biomass and Bioenergy, 31, 563–568. https://doi.org/10.1016/j.biombioe.2007.03.001

Faridi, J. A. (2017). Preparation of char based catalyst and its application for differrent purposes (A. Gasparella, M. Baratieri, F. Patuzzi, & U. Rashid (eds.)). PhD in Sustainable Energy and Technologies Dissertation, Faculty of Science and Technology, Universita Liedia de Bulsan.

Ghorbani-Choghamarani, A., Taherinia, Z., & Tyula, Y. A. (2022). Efficient biodiesel production from oleic and palmitic acid using a novel molybdenum metal–organic framework as efficient and reusable catalyst. Scientific Reports, 12(10338), 1–12. https://doi.org/10.1038/s41598-022-14341-4

Han, B., Yin, F., Liu, S., Zhao, X., Liu, J., Wang, C., Yang, H., & Zhang, W. (2019). Optimization of oleic acid esterification for biodiesel production using Brønsted acidic ionic liquid as a catalyst. Chiang Mai Journal of ScienceSci, 46(4), 714–726. http://epg.science.cmu.ac.th/ejournal/

Ibrahim, N. A., Rashid, U., Hazmi, B., Moser, B. R., Alharthi, F. A., Rokhum, S. L., & Ngamcharussrivichai, C. (2022). Biodiesel production from waste cooking oil using magnetic bifunctional calcium and iron oxide nanocatalysts derived from empty fruit bunch. 1–42. https://www.sciencedirect.com/science/article/pii/S0016236122003908

Kumawat, M. K., & Rokhum, S. L. (2022). Biodiesel production from oleic acid using biomass-derived sulfonated orange peel catalyst. Frontiers in Catalysis, 2(914670), 1–12. https://doi.org/10.3389/fctls.2022.914670

Kushwaha, T., Ao, S., Ngaosuwan, K., Assabumrungrat, S., Gurunathan, B., & Rokhum, S. L. (2023). Esterification of oleic acid to biodiesel using biowaste-based solid acid catalyst under microwave irradiation. Environmental Progress and Sustainable Energy, 42(6). https://doi.org/10.1002/ep.14170

Kusmiyati, & Sugiharto, A. (2010). Production of biodiesel from oleic acid and methanol by reactive distillation. Bulletin of Chemical Reaction Engineering & Catalysis (BCREC), 5(1), 1–6. http://bcrec.undip.ac.id

Lucena, I. L., Silva, G. F., & Fernandes, F. A. N. (2008). Biodiesel production by esterification of oleic acid with methanol using a water adsorption apparatus. Industrial & Engineering Chemistry Research, 18(47), 6885–6889. https://doi.org/10.1021/ie800547h

Maafa, I. M. (2022). Biodiesel synthesis from high free-fatty-acid chicken fat using a scrap-tire derived solid acid catalyst and KOH. In C. Delattre (Ed.), Polymers 14(643). https://doi.org/10.3390/polym14030643

Mahdavi, M., Abedini, E., & Darabi, A. hosein. (2015). Biodiesel synthesis from oleic acid by nano-catalyst (ZrO2/Al2O3) under high voltage conditions. RSC Advances, 5(68), 55027–55032. https://doi.org/10.1039/C5RA07081C

Maryam, U. A., Maspalma, G. A., Manu, J. M., & Hamid, M. B. (2021). Production and optimization of biodiesel from palm fatty acid distillate and oleic acid using response surface methodology approach. Journal of Chemical Society of Nigeria, 46(1), 36–48. https://journals.chemsociety.org.ng/index.php/jcsn/article/view/582/639

Moradi, P., Saidi, M., & Najafabadi, A. T. (2021). Biodiesel production via esterification of oleic acid as a representative of free fatty acid using electrolysis technique as a novel approach: Non-catalytic and catalytic conversion. Process Safety and Environmental Protection, 147, 684–692. https://doi.org/10.1016/j.psep.2020.12.032

Naeem, A., Khan, I. W., Farooq, M., Mahmood, T., Ud Din, I., Ghazi, Z. A., & Saeed, T. (2021). Kinetic and optimization study of sustainable biodiesel production from waste cooking oil using novel heterogeneous solid base catalyst. Bioresource Technology, 328(124831), 1–8. https://doi.org/10.1016/j.biortech.2021.124831

Narkhede, N., & Patel, A. (2013). Biodiesel production by esterification of oleic acid and transesterification of soybean oil using a new solid acid catalyst comprising 12-tungstosilicic acid and zeolite Hβ. Industrial & Engineering Chemistry Research, 52, 13637−13644. https://doi.org/10.1021/ie402230v

Nata, I. F., Irawan, C., & Lee, C.-K. (2017). Catalytic performance of sulfonated carbon-based solid acid catalyst on esterification of waste cooking oil for biodiesel production. Journal of Environmental Chemical Engineering (JECE), 1–19. https://doi.org/10.1016/j.jece.2017.04.029

Oyedoh, E. A., Okoduwa, G. U., Madojemu, G. O., & Akhabue, C. E. (2022). Production of biodiesel from the transesterification of waste cooking oil using biobased sulphonated catalyst prepared from coconut shells. Journal of Applied Science and Environmental Management (JASEM), 26(12), 1977–1987. https://doi.org/10.4314/jasem.v26i12.12

Pang, H., Yang, G., Li, L., & Yu, J. (2021). Esterification of oleic acid to produce biodiesel over 12-tungstophosphoric acid anchored two-dimensional zeolite. Chemical Research in Chinese Universities, 37, 1072–1078. https://doi.org/10.1007/s40242-021-1152-0

Patel, A., Brahmkhatri, V., & Singh, N. (2013). Biodiesel production by esterification of free fatty acid over sulfated zirconia. Renewable Energy, 51, 227–233. https://doi.org/10.1016/j.renene.2012.09.040

Rahma, F. N., & Hidayat, A. (2023). Biodiesel production from free fatty acid using ZrO2/bagasse fly ash catalyst. International Journal of Technology, 14(1), 206–218. https://doi.org/10.14716/ijtech.v14i1.4873

Rani, K. N. P., Neeharika, T. S. V. R., Vardhan, G. H., Kumar, T. P., & Devi, B. L. A. P. (2020). The kinetics of the esterification of free fatty acids in jatropha oil using glycerol based solid acid catalyst. European Journal of Sustainable Development Research (EJSDR), 4(2), 1–11. https://doi.org/10.29333/ejosdr/7594

Sawitri, D. R., & Budiman, A. (2016). Kinetics study of free fatty acids esterification for biodiesel production from palm fatty acid distillate catalysed by sulfated zirconia. ARPN Journal of Engineering and Applied Sciences, 11(16), 9951–9957. http://www.arpnjournals.com

Silva, M. G., Oliveira, G. S., Carvalho, J. C. R., Nobre, L. R. P., Deus, M. S., Jesus, A. A., Oliveira, J. A., & Souza, D. F. S. (2019). Esterification of oleic acid in a semi-batch bubble reactor for biodiesel production. Brazilian Journal of Chemical Engineering, 36(1), 299–308. https://doi.org/10.1590/0104-6632.20190361s20180185

Suwannakarn, K., Lotero, E., Ngaosuwan, K., & Goodwin, J. G. (2009). Simultaneous free fatty acid esterification and triglyceride transesterification using a solid acid catalyst with in situ removal of water and unreacted methanol. Ind. Engineering Chemical Research, 48, 2810–2818. https://doi.org/10.1021/ie800889w

Taufiq, A., Arista, S., Sutrisno, B., Feng, Y., Hu, J., Wang, F., Li, W., & Yi, M. (2018). Kinetic study on the esterification of palm fatty acid distillate (PFAD) using heterogeneous catalyst. IOP Conf. Series: Materials Science and Engineering (ICGSCE 2017), 358(012069), 1–7. https://doi.org/10.1088/1757-899X/358/1/012069

Yadav, G., Yadav, N., & Ahmaruzzaman, M. (2022). Microwave-assisted synthesis of biodiesel by a green carbon - based heterogeneous catalyst derived from areca nut husk by one-pot hydrothermal carbonization. Scientific Reports, 12(21455), 1–14. https://doi.org/10.1038/s41598-022-25877-w

Zhang, B., Wang, X., Tang, W., Wu, C., Wang, Q., & Sun, X. (2023). Carbon-based solid acid catalyzed esterification of soybean saponin-acidified oil with methanol vapor for biodiesel synthesis. Sustainability, 15(13670), 1–15. https://doi.org/10.3390/ su151813670

Zhang, Q., Wei, F., Zhang, Y., Wei, F., Ma, P., Zheng, W., Zhao, Y., & Chen, H. (2017). Biodiesel production by catalytic esterification of oleic acid over copper (II)-alginate complexes. Journal of Oleo Science, 66(5), 491–497. https://doi.org/10.5650/jos.ess16211

Zubir, M. I. Bin. (2009). Esterification of oleic acid with ethanol by using tungstated zirconia: Kinetic and modeling study (C. S. Yee (ed.)) [Degree of Bachelor of Chemical Engineering, Faculty of Chemical and Natural Resources Engineering, Universiti Malaysia Pahang]. https://core.ac.uk/download/pdf/159177489.pdf